In Vivo Mapping of Brain Elasticity in Small Animals Using Shear Wave Imaging

Emilie Macé, *Member, IEEE,* Ivan Cohen, Gabriel Montaldo, *Member, IEEE,* Richard Miles, Mathias Fink, *Member, IEEE,* and Mickael Tanter, *Member, IEEE*

***Abstract*—A combination of radiation force and ultrafast ultrasound imaging is used to both generate and track in the brain the propagation of a shear wave whose local speed is directly related to stiffness, characterized by the dynamic shear modulus G. When performed on trepanated rats, this approach called Shear Wave Imaging (SWI) provides 3D brain elasticity maps reaching a spatial resolution of 0.7 mm x 1 mm x 0.4 mm with a good reproducibility (< 13 %). The dynamic shear modulus of brain tissues exhibits values in the 2-25 kPa range with a mean value of 12 kPa and is quantified for different anatomical regions. The anisotropy of the shear wave propagation is studied and the first in vivo anisotropy map of brain elasticity is provided. The propagation is found to be isotropic in three gray matter regions but highly anisotropic in two white matter regions. The good temporal resolution (~10ms per acquisition) of SWI also allows a dynamic estimation of brain elasticity to within a single cardiac cycle, showing that brain pulsatility does not transiently modify local elasticity. SWI proves its potential for the study of pathological modifications of brain elasticity both in small animal models and in clinical intra-operative imaging.**

***Index Terms*—Anisotropy, brain, elasticity, Shear Wave Imaging, ultrasound.**

I. Introduction

ABNORMALtissues tissues are known to have different mechanical properties from healthy tissues. This characteristic is widely used by clinicians on accessible organs to detect tumors or lesions through manual palpation. Though direct "palpation" of the brain is feasible during certain neurosurgical procedures, it remains extremely limited. Quantitative assessment of brain elasticity in vivo would be of great interest for many applications in neurology and neurosurgery. For diagnosis, it could help improve detection of tumors. In neurosurgery, real-time brain elasticity imaging could provide a new intra-operative tool for lesion localization and margin assessment. In fundamental research on brain pathologies such as neurodegenerative diseases, it could help understand the mechanisms of development and provide follow-up of drug treatment efficiency on small animal models. In basic research on traumatic brain injury, biomechanical studies need a precise estimation of mechanical parameters of brain tissues for numerical models.

Brain viscoelasticity has been investigated extensively in vitro with rheological experiments [1]. However, a large discrepancy is observed in the literature for the values of dynamic shear modulus of brain tissues. This lack of consistency can be attributed to the variety of sample types, strain rates, methods and protocols used. For example, for shear oscillatory testing of white matter at 200 Hz, the values available in the literature for the storage modulus Gd range from 1 kPa to 12 kPa [2].

In recent years, brain elasticity has also been imaged in vivo by Magnetic Resonance Elastography (MRE) both on humans [3-9] and on small animals [10-12]. MRE [13] is a non invasive elasticity imaging technique based on a phase-sensitive MR sequence that detects the propagation of shear waves generated by an external vibrator. However, the spatial resolution of this technique remains limited because it is intrinsically linked to acquisition time. To obtain a clinically relevant resolution, the acquisition time is very long (several minutes per acquisition) limiting its use as an intra-operative tool or as a routine test for research on small animals. The development of a real-time and accessible brain elasticity imaging modality, with high enough resolution to provide detailed mapping of the brain would be a useful complement to MRE in neurosciences.

Ultrasound transient elastography by Shear Wave Imaging (SWI) is a promising candidate. Ten years ago, the concept of Transient Elastography [14-17] was proposed to provide the advantage of quantitative elasticity imaging combined with real-time and freehand capabilities. The key point of this approach is the use of an ultrafast ultrasound acquisition imaging system (several thousand frames per second), which enables the real-time visualization of transient shear waves propagating in the human body. For palpating tissues,

Manuscript received April 20, 2010, revised July 15, 2010. This work was supported in part by the French National Insitute on Health and Medical Research (INSERM) and by the National Center on Scientific Research (CNRS).

E. Macé, G.Montaldo, M. Fink and M. Tanter are with the Institut Langevin, ESPCI ParisTech, Paris, France (e-mail: emilie.mace@espci.fr; gabriel.montaldo@espci.fr; mathias.fink@espci.fr; mickael.tanter@espci.fr; phone: +33140794452; fax: +33140794468).

I. Cohen and R. Miles are with the Cortex and Epilepsy Laboratory, Hopital Pitié-Salpétrière, Paris France (e-mail: ivan.cohen@upmc.fr; rmiles@chups.jussieu.fr).

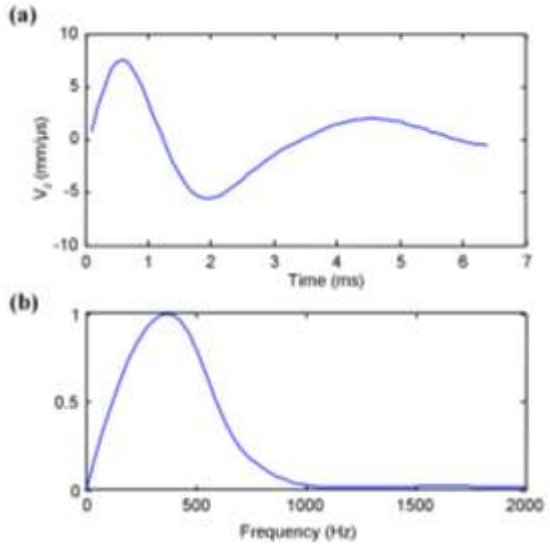

Fig. 2. Axial velocity profile (a) and frequency spectrum (b) measured in a pixel of the image induced by the propagation of the shear wave.

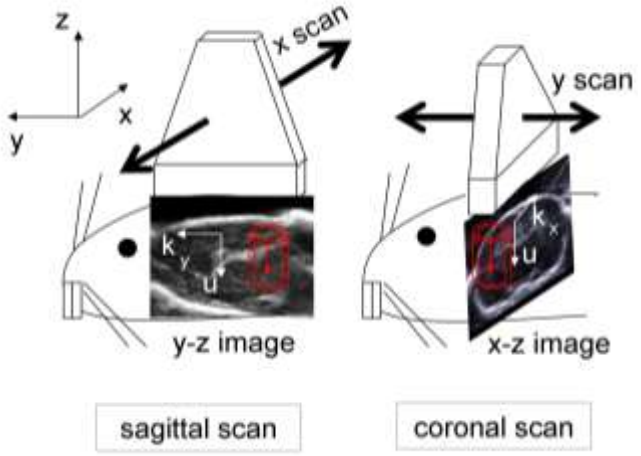

Fig. 3. Schematic of the two scans performed, k is the wave vector measured and u the polarization of the shear wave. Sagittal scan: the shear wave is polarized along z and its propagation along y is imaged. Coronal scan: the shear wave has the same polarization but its propagation along x is imaged.

Transient Elastography initially used external vibrators similar to the ones used in MRE, but evolved into a much more convenient technique, SWI, using the radiation force of an ultrasonic focused beam [18, 19].

SWI was proved of clinical interest for the improvement of diagnosis in breast cancer [20] and its feasibility was demonstrated on other organs such as the liver [21], muscle [22], arteries [23] and cornea [24]. The key asset of SWI compared with other techniques lies in the ultrafast imaging of the transient propagation of a shear wave remotely induced by ultrasonic beams. The speed of this wave is driven by the local dynamic shear modulus of tissues. The main advantages offered by SWI compared to MRE are its higher spatial and temporal resolutions (several quantitative elasticity maps per second) as well as its low cost and high accessibility. However, because of high absorption and diffraction effects induced on the ultrasonic wavefield during transcranial propagation, SWI of the brain currently has to be performed invasively after trepanation.

In this initial work, the ability of SWI to quantitatively map brain elasticity is demonstrated in vivo on trepanated rats. The potential of this technique to estimate the anisotropy of brain mechanical properties is explored. Moreover, the ability of this technique to realize several elasticity measurements within one single cardiac cycle is used to investigate potential dynamic elasticity changes in brain tissues due to pulsatility.

II. Materials and Methods

A. Experimental setup

This protocol was performed at Pitié Salpêtrière Hospital (Paris, France). It follows local regulations on small animal experimentation and is in accordance with international standards on animal welfare. This study encloses the results obtained on five adult Sprague Dawley rats weighing approximately 500g. Rats were deeply anesthetized either by an injection of Ketamine Xylazine (2 rats) or with isoflurane (4% for induction and 2% for maintenance) in O2 enriched air (3 rats). The head was placed in a stereotaxic frame and the upper surface of the cortex was exposed through a 13 mm x15 mm cranial window (typically from bregma +5 mm to bregma -8 mm in the anterior-posterior axis). A wall was built around the opening by applying several layers of dental cement and the cavity was filled with an isotonic aqueous solution of xanthan gum (0.3%). A conventional ultrasonic linear probe (Vermon, 8MHz central frequency, 256 elements) was positioned 5 mm above the brain surface either in the sagittal plane or the coronal plane. Acoustic contact between the probe and the brain was ensured by the viscous xanthan gum solution. Only the 128 first elements of the probe were used to image the rat brain. The probe was controlled by a motorized arm which allowed the scanning of the whole brain volume with micrometric precision. The probe was connected to an ultrafast ultrasound scanner (AixplorerT.M., SuperSonic Imagine, Aix en Provence, France). This system provided 2D images with a very high frame rate reaching up to 20 kHz. The software based architecture of the scanner enabled full programming of custom transmit/receive ultrasonic sequences. The experimental setup is illustrated in Fig 1.

B. The Shear Wave Imaging technique

A detailed description of the SWI technique can be found in [19, 20].

For shear wave generation, a burst of ultrasound (typically 100µs duration) is transmitted by the conventional probe and focused on a small zone of the brain, inducing a typical ~100 µm tissue displacement along the ultrasonic beam direction at the focal point. By moving the ultrasound beam supersonically in depth, a line source is excited and a 3D cylindrical shear wave is generated. This shear wave exhibits a frequency spectrum in the low kHz range and propagates in the brain at a velocity that depends on tissue elasticity (from 1 to 20 m/s for

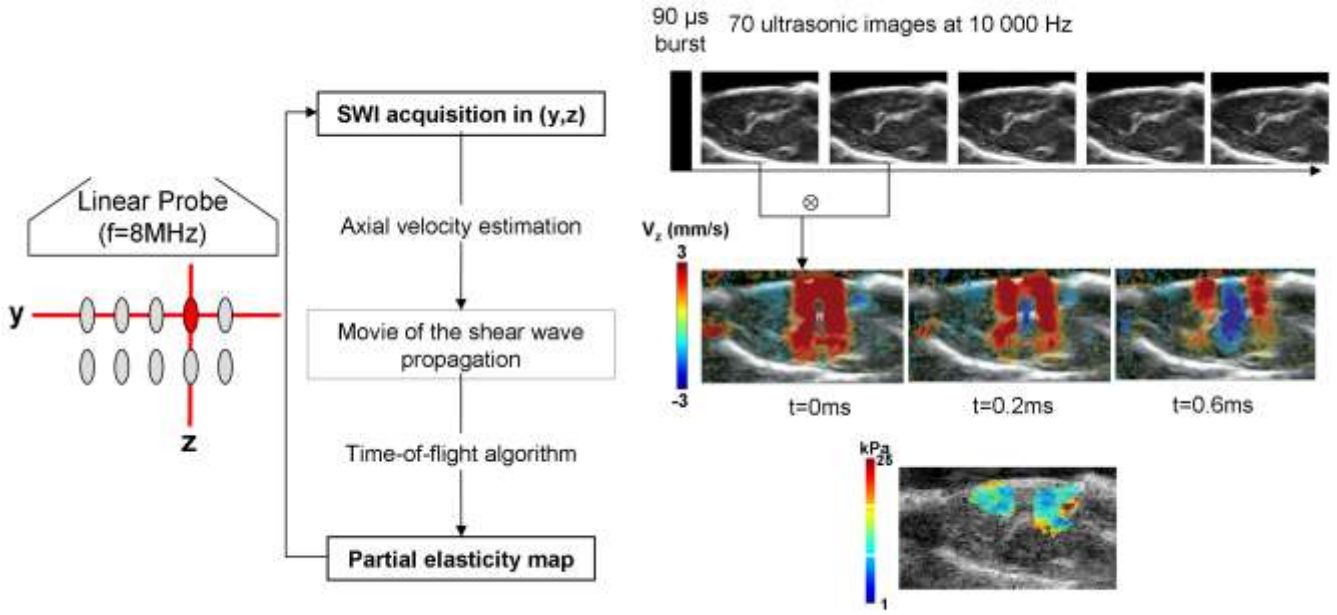

Fig. 4. Illustration of a SWI sequence at a position (y,z) from the acquisition to the reconstruction of a partial elasticity map. To reconstruct a complete elasticity map for a brain slice, 10 SWI sequences were performed at different focal points (y,z) and the partial elasticity maps were combined.

soft tissues).

The propagation of the shear wave is imaged with ultrasound at a very high frame rate (> 5000 Hz) using the same probe. The axial component of tissue particle velocity Vz (see Fig 2a) can be measured in each point of the imaging plane by cross-correlations between two consecutive ultrafast ultrasound images [19].

A plane wave propagating in a homogeneous medium following a rheological law $\vec{\sigma}(\omega) = G^*(\omega)\vec{\varepsilon}(\omega)$, where G* is the complex dynamic shear modulus $G^* = G_d + iG_l$, propagates at a phase speed c given by ([25]):

$$c(\omega) = \sqrt{\frac{2}{\rho}\frac{{G_d}^2 + {G_l}^2}{G_d\left(1+\sqrt{1+\left(\frac{G_l}{G_d}\right)^2}\right)}} \quad (1)$$

Under the approximation of low viscosity, and the equation (1) becomes:

$$c(\omega) = \sqrt{\frac{G_d}{\rho}} \quad (2)$$

We define a shear modulus estimator $\hat{G} = \rho c(\omega)^2$ in order to give a magnitude in kPa. However, as the viscosity is non-negligible in the brain, one should keep in mind that the magnitude measured by SWI is the group shear velocity.

Assessing the complete frequency dependency $c(\omega)$ of the shear wave speed in a single pixel of the final image is to date an unachievable task due to limited signal to noise ratio. Therefore, only the group speed of the shear wave c^g (i.e. the wave speed of the wave packet) is estimated in each pixel from the axial velocity of tissues Vz. This local group speed is measured using a dedicated time-of-flight algorithm similar to [26] that computes the time needed for the wave to propagate between two neighboring points separated by 1 mm (i.e. 5 pixels). In a first approximation, c^g corresponds to the phase speed of the shear wave at the dominant frequency component ω_0 of the shear wave packet. As a result, the estimator of the shear modulus measured by SWI can be expressed as followed:

$$\hat{G} = \rho c(\omega_0)^2 \quad (3)$$

Applying the time of flight algorithm to each pixel of the 2D image sequence of shear wave propagation enables the assessment of a complete map of the value of $\hat{G}$ characterizing the local mechanical properties of the tissue.

C. Imaging sequences

1) Bmode scan

For each animal, two standard ultrasonic scans of the brain were first acquired, one in the coronal plane and one in the sagittal plane. These scans were performed with the conventional 2D B-mode of the AixplorerT.M. scanner. The probe was moved with a 200 µm spatial step along the brain using the motorized arm.

2) SWI mapping scan

One SWI sequence consisted of acquiring 70 ultrasound images at a frame rate of 10,000 Hz immediately after generating a shear wave using a 90 µs supersonic shear source

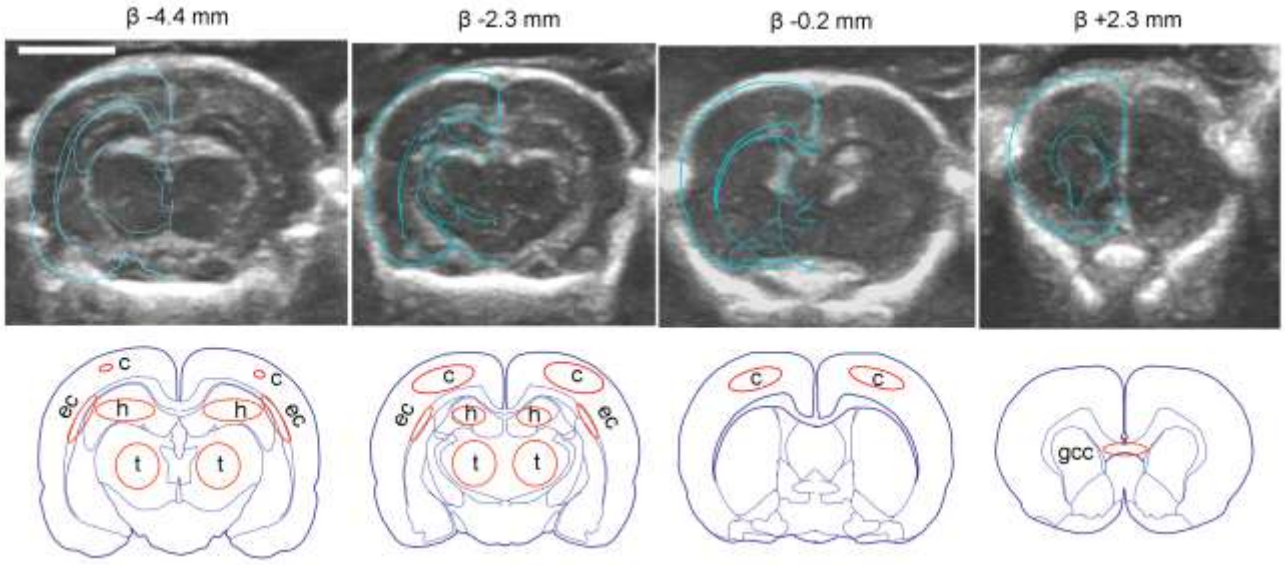

Fig. 5. Top – Bmode images registered with the anatomy (blue lines) from Paxinos and Watson atlas of the rat brain [26]. Bottom – Limits of the five ROIs - hippocampus (h), cortex (c), thalamus (t), external capsule (ec), genu of corpus callosum (gcc) superposed on the atlas. Bar =5 mm

[19] focused on a line of 4 mm in depth. The acquisition time for one SWI sequence was < 10ms. Because the velocity of the shear wave cannot be computed at the focal point, one SWI sequence gives only a partial elasticity map of the slice. As a result, 10 SWI acquisitions were performed at different positions in the imaging plane in order to reconstruct a complete elasticity map of the brain slice (see Fig 4). As explained before, the value of dynamic shear modulus measured depends on the frequency spectrum of the shear wave. In this experiment, the dominant frequency component of the generated shear wave packet is ~400 Hz and the bandwidth of the spectrum is large (~100%) as shown on Fig 2b.

It is important to point out that the shear wave generated by the radiation force is cylindrical [19]. In other words, it is planar in the imaging plane and only diffracting in the elevation direction (direction perpendicular to the imaging plane). The polarization vector is always directed along the depth axis (z) but the propagation direction that we measure is in the plane of the transducer array. If the probe is set in the sagittal (yz) plane, we measure a shear wave propagating along the anterior-posterior (y) axis of the brain (Fig 3a). Conversely, if the probe is in the coronal (xz) plane, we measure a shear wave propagating along the right-left (x) axis of the brain (Fig 3b). If the elasticity tensor of the brain is not isotropic then shear wave velocity values are expected to be different in these two configurations.

Four animals were scanned in the SWI mode. Both a sagittal and a coronal SWI scan were performed on these animals, with a scanning step of either 200µm (2 animals) or 400µm (2 animals).

3) Dynamic SWI sequence

On the fifth animal, a dynamic SWI sequence was performed to estimate the changes of elasticity in the brain induced by blood flow pulsatility. At a given position (y,z) in a selected sagittal slice, a 90µs focused ultrasonic beam was transmitted and the generated shear wave was imaged at 5000 Hz. This SWI acquisition was repeated 15 times in 270 ms which corresponds to one and a half cardiac cycle of the rat. The electrocardiogram and the reference pulses of the ultrasonic images were recorded with a differential amplifier. This experiment was repeated 10 times on the same slice in order to obtain statistical values.

D. Image Processing

1) Reconstruction of 3D elasticity maps

For each brain slice scanned, the quantitative elasticity map was reconstructed using Matlab software. For that, as illustrated in Fig 4, the ultrafast ultrasonic images acquired for each SWI acquisition were processed to measure tissue velocity and then to measure shear wave group velocity with the time-of-flight algorithm, giving a partial elasticity map. Partial maps from the 10 spatially dispersed SWI acquisitions were then combined to obtain the complete elasticity map of the brain slice.

We took into account reflections and/or low SNR that could lead to artefacts on the elasticity map by implementing:

- a directional filter applied on the velocity field that rejects the reflections of the shear wave on boundaries before the time-of-flight algorithm. This directional filter consists of a bi-dimensional Fourier transform of the velocity field $V_z(x,t)$ for each depth (z). Since we know in which direction the generated shear wave propagates, a filter is applied on this spectrum to eliminate wave vectors kx corresponding to propagation in the opposite direction. A new velocity field $V_z(x,z,t)$ is obtained by an inverse Fourier transform that is then used in the time-of-flight algorithm.
- a rejection of pixels with low SNR. To estimate the shear velocity in each pixel, the time-of-flight algorithm calculates

the correlation function between two displacement vectors u(t) separated by a distance of 1 mm. If the SNR is poor, the correlation coefficient between these two vectors is low (typically <0.7), meaning that the estimation of the shear velocity is not possible, and the pixel is rejected. The quality of the correlation is also used to optimize the combination of the partial elasticity maps.

The spatial resolution of this 2D elasticity map is of the order of 700 µm by 1 mm and the spatial sampling is 170 µm by 200 µm. This can be justified as following. The spatial resolution and sampling of the ultrasonic images is 0.17 mm in depth and 0.2 mm along the transducer array for the 8 MHz probe used. The velocity estimation is based on autocorrelations along depth using a 4 sample window with an overlap of 3 samples. It generates velocity images with the same sampling (0.17 mm) but a resolution of 0.7 mm in depth. The time of flight is then estimated along the transducer array axis between two points spaced from 5 samples with an overlap of 4 samples, which gives the same sampling (0.2 mm) but a resolution of 1 mm. In the third direction, the sampling is given by the scanning step (i.e. 200 µm or 400µm) and the resolution by the focusing parameters of the probe, 400µm in this case.

Medical imaging software AMIDE was used for 3D image reconstruction (http://amide.sourceforge.net/). Each SWI scan of the brain resulted in a stack of 2D elasticity maps that were interpolated with AMIDE to reconstruct a 3D elasticity map. A 3D median filtering (kernel size 3) was applied. In this paper, to help visualizing 3D elasticity maps, we chose to always present coronal sections, whether the scan was performed in the coronal or the sagittal plane

2) Registration and segmentation

For each animal, two 3D Bmode image (sagittal and coronal) and two 3D elasticity maps (sagittal and coronal) were obtained. The B-mode images and the 3D elasticity maps acquired in the same orientation do not need to be registered. The problem was to register the images from different orientations and from different animals. This task has been simplified by applying the following protocol:

- Animals of the same sex (males) and weight (500g) were chosen to minimize the variations of head and brain size.
- The head was placed in the stereotaxic frame with the same coordinates which enabled to always have the head in a similar position for all animals.
- The bregma point was identified before trepanation, and the ultrasonic probe was aligned in respect with this point to ensure similar scans for all animals.

As a consequence, only a small misalignment right-left (x axis) and top-bottom (z axis) is observed between images that was estimated less than 1 mm. This misalignment was corrected manually using AMIDE software. For that, we registered the B-mode images on which some anatomical structures were easy to identify (hippocampus, ventricles and thalamus) using a rigid registration. After registration, two average elasticity maps, one for the sagittal scan and one for the coronal scan, were generated from the mean values over the four animals. In the results section, variance statistics are given as the standard deviation of the mean (σ) across the four animals.

In order to quantify the shear modulus in different brain regions, segmentation was performed on the average elasticity maps. For that, an atlas of the rat brain (Paxinos et al) was transferred into AMIDE and registered (rigid registration) with the Bmode image based on the known stereotaxic coordinates of the bregma. Five regions of interest (ROIs) were segmented, three in gray matter structures (the cortex, the thalamus and the hippocampus) and two in white matter structures (the genu of the corpus callosum and the external capsule). We manually selected 3D ellipsoid ROIs smaller than the brain region considered in order to minimize the impact of misregistration between the atlas and the Bmode image on the quantification. The result of the segmentation process for four coronal slices is presented in Fig 5.

TABLE I
ELASTIC PROPERTIES OF DIFFERENT BRAIN REGIONS

ROI	Sagittal Scan $\hat{G}$(kPa)	Coronal Scan $\hat{G}$(kPa)	P-Value	Size (mm^3)
whole brain	12.3 ± 0.7	11.6 ± 1.5	0.146	444.2
cortex	12.9 ± 1.3	13.3 ± 2.9	0.795	29.3
hippocampus	8.6 ± 1.2	10.0 ± 1.0	0.115	16.7
thalamus	12.4 ± 1.5	10.2 ± 0.5	0.030	35.6
genu of cc.	21.4 ± 5.9	7.8 ± 2.0	0.013	3.5
extenal capsule	14.9 ± 1.9	25.3 ± 5.7	0.005	8.0

For each ROI, mean value and standard deviation of $\hat{G}$ over 4 animals for sagittal and coronal scans, p-value between sagittal and coronal scans and size of the ROI in mm^3.

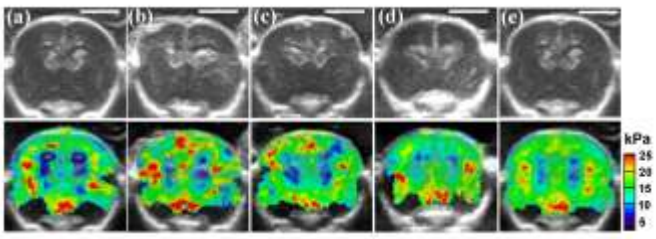

Fig. 6. Reproducibility over 4 animals for a coronal brain slice (β -0.5 mm). a) Elasticity maps (from sagittal scan) obtained for the four animals. b) Averaged elasticity map over 4 animals obtained after registration. Bar = 5 mm.

III. Results

A. Anatomy

A conventional B-mode ultrasonic scan of the rat brain allows the identification of the main anatomical structures such as the hippocampus and thalamus (see Fig 5 and Fig 7). The field of view after craniotomy extended from the root of the olfactory bulbs to the posterior part of the midbrain before the cerebellum. The resolution achieved was of the order of the ultrasonic wavelength -170x200µm²- for the 8MHz central frequency probe used.

B. Elasticity of the rat brain

The mean value and standard deviation over the 4 animals was quantified for the whole brain and in the five segmented ROIs. The results are listed in Table 1.

For the sake of clarity, only the results obtained with sagittal scans are discussed in this section. The stiffness values were found to be in the 2-25 kPa range. The mean stiffness value obtained over the whole brain was $\hat{G}$=12.3 kPa. The variation of this value over the 4 animals was lower than 6% and similar spatial distribution of the elastic properties were observed on maps from different animals, as illustrated in Fig 6 for a selected coronal slice (β -0.5 mm).

Fig 7 presents the average 3D elasticity map over 4 animals for coronal slices every 500 µm as well as the corresponding anatomical ultrasonic image. It is clear that some brain structures exhibit differences in elasticity values. In particular, in all animals, the forebrain (rostral part of the brain) was found to be stiffer ($\hat{G}$ = 13.2 +/- 0.7 kPa) than the midbrain (between the forebrain and the cerebellum) ($\hat{G}$ = 11.7 +/- 0.6 kPa) with a good significance level (p-value=0.017).

Given the spatial resolution achieved, a more detailed analysis is possible in the five ROIs illustrated in Fig 5. The results are reported in Fig 8 (gray bars). The hippocampus has the lowest shear modulus. The cortex and the thalamus exhibit similar stiffness values, of the order of the mean value in the brain. Higher mean shear modulus values were found in the two white matter regions, the genu of the corpus callosum and the external capsule.

C. Anisotropy of shear wave propagation

The elasticity maps shown in the previous section were obtained from sagittal SWI scans. As it was explained previously, the propagation along y (anterior-posterior axis) of the shear wave is measured with sagittal scans whereas its propagation along x (left-right axis) is measured with coronal scans. To study a possible anisotropy of the shear wave propagation, the 3D average elasticity maps $\hat{G}s$ (x,y,z) and $\hat{G}c$ (x,y,z) obtained from sagittal and coronal scans respectively were compared. When looking at the same coronal section (β -4.2 mm) of these two maps, as shown on Fig 9, it is clear that they are very different.

In an attempt to quantify this anisotropy, a relative index Δ characterizing the difference between shear wave group speeds along coronal and sagittal plane directions, c_{cor} and c_{sag} respectively, was computed. This index describes the local relative shear anisotropy:

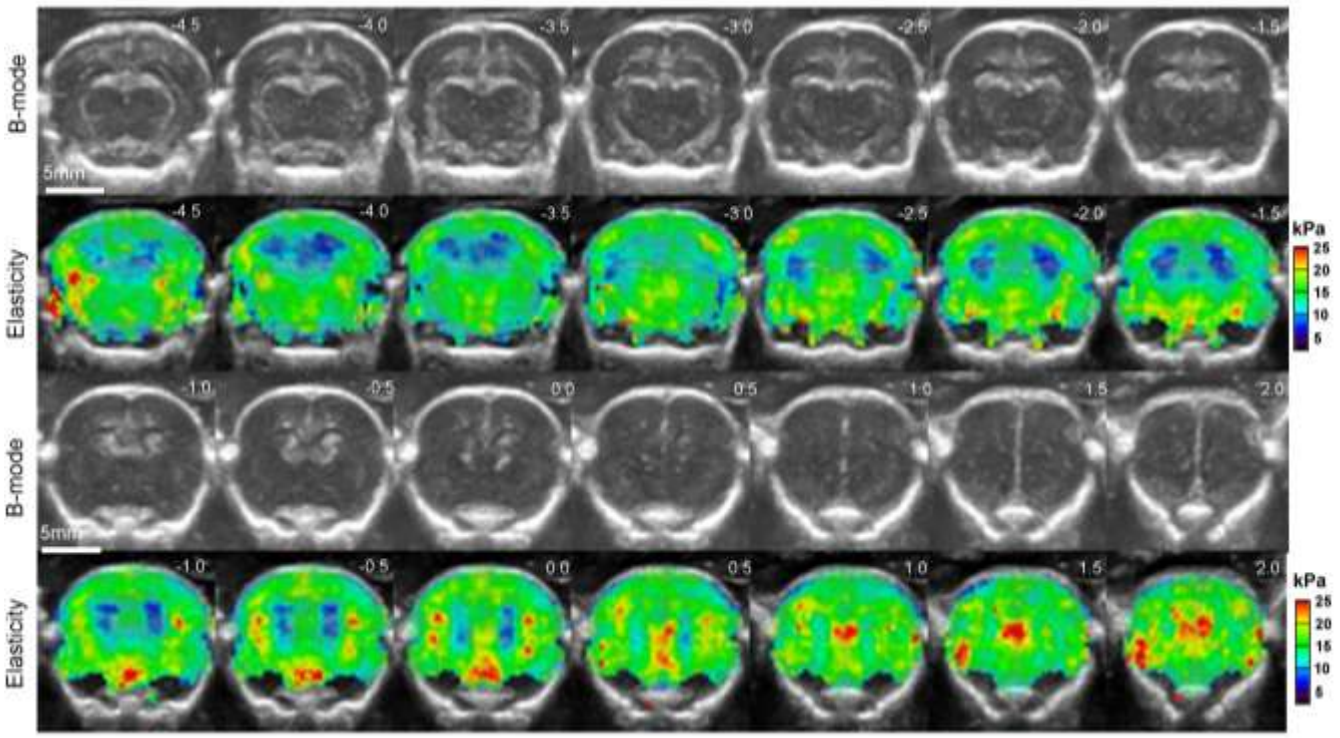

Fig. 7. Bmode images (top) and corresponding averaged elasticity maps (bottom) reconstructed in the coronal plane from the sagittal SWI scan of the rat brain. The zero was set at the position of the bregma. All elasticity maps are represented with the same scale: from 2 to 25 kPa for the absolute value of the dynamic shear modulus $\hat{G}$.

$$\Delta = \frac{c_{cor} - c_{sag}}{c_{sag}} \quad (4)$$

By definition, Δ is positive if the shear wave propagates faster in the coronal plane and negative if the shear wave propagates faster in the sagittal plane.

A map of the relative shear anisotropy index Δ is presented for the same coronal section (β -4.2 mm) in Fig 9. The map shows that the external capsule is anisotropic. In this white matter structure, the shear wave propagates faster in the coronal plane.

The statistical values obtained for $\hat{G}$ in different brain regions over the 4 animals with coronal scans are also reported in Table **Erreur ! Source du renvoi introuvable.** and compared with the values from sagittal scans in Fig 8 (white bars). The brain was not found significantly anisotropic on average (p-value = 0.146). Similarly, no significant difference was observed between the two orientations in the cortex (p-value = 0.795=1) and in the hippocampus (p-value = 0.115). In the thalamus, the two groups are significantly distinct (p-value = 0.0299 <5%) but the mean values of $\hat{G}$ are close, showing an anisotropy but only small in this gray matter region. In the two white matter regions, the external capsule and the genu of the corpus callosum, the mean values were distinct and this difference was significant (p-values = 0.013 and 0.005 respectively, <5%) which means that those ROIs are highly anisotropic. It is noticeable that the direction of the anisotropy is opposite for the two white matter regions: the shear wave propagates faster in the coronal plane in the external capsule but faster in the sagittal plane in the genu of corpus callosum.

D. Dynamic changes in brain elasticity

The elastic properties of some biological tissues like artery walls are known to be transiently modified by cardiac pulsatility [23]. Thanks to its high temporal resolution, SWI allowed the imaging of such rapid changes in elasticity. To estimate this effect in the brain, the shear wave speed was measured several times in a cardiac cycle using the dynamic SWI sequence described earlier.

Within a dynamic SWI sequence, 15 SWI acquisitions were performed at different time of the cardiac cycle. Each acquisition gave a partial elasticity map of the brain slice, from which a mean value of stiffness is obtained in a ROI located in the hippocampus. This dynamic SWI sequence was then repeated 10 times at the same position on the same brain slice, resulting in 10 estimations of stiffness in the ROI for each temporal point of the electrocardiogram. The mean (marker) and standard deviation (error bar) of $\hat{G}$ across the 10 estimations are presented in Fig 10 with the corresponding electrocardiogram. The mean value found in the ROI was 8.7 kPa with a standard deviation of the mean over time of 0.5 kPa. The standard deviation of $\hat{G}$ (i.e. error bar) is on average 2.7 kPa. No noticeable change in elasticity was observed during the passage of the arterial pulse in this region of the brain.

IV. Discussion

In this study, ultrasound elasticity mapping of the brain using the Supersonic Wave Imaging approach is demonstrated in vivo on trepanated rats. The shear modulus is found to be in the 2-25 kPa range and is quantified in different anatomical regions of the brain. Reproducibility of the technique is found to be very good (< 13 %) and similar spatial distributions of elastic properties are found across all rats (N=4). The technique is also proved to be capable of estimating the shear anisotropy of the mechanical properties of tissue and measuring these properties dynamically within one cardiac cycle.

The spatial resolution of the elasticity maps, of the order of 0.7 mm x 1 mm x 0.4 mm is to our knowledge the highest achieved in vivo to date. This good resolution enables the measurement of quantitative elasticity values for different brain regions. More importantly, the resolution of this new brain elastography technique could be further improved by increasing the central frequency of the ultrasonic array. Higher frequency ultrasound means higher resolution for the ultrasound images but also higher frequencies generated by the radiation force. These two effects would lead to an improved time-of-flight estimation and a better spatial resolution for the resulting maps. The process of registration and segmentation could also be improved by using better resolved ultrasonic images. The limited penetration depth at higher frequencies would not be an issue given the small size of the rat brain (<1.5cm along z). For all these reasons, future experiments are being planned with 15 to 25 MHz probes.

Comparison with the literature is not straightforward because in reality tissues are viscous and the shear modulus depends strongly on the frequency. For example, it has been demonstrated in the human liver that the shear modulus can increase by a factor of two between 100Hz and 400Hz [27]. Moreover, contrary to MRE, the shear wave generated in SWI is not monochromatic but exhibits a large frequency spectrum (centered on 400 Hz in this experiment). However, in a first approximation the present quantification can be considered as

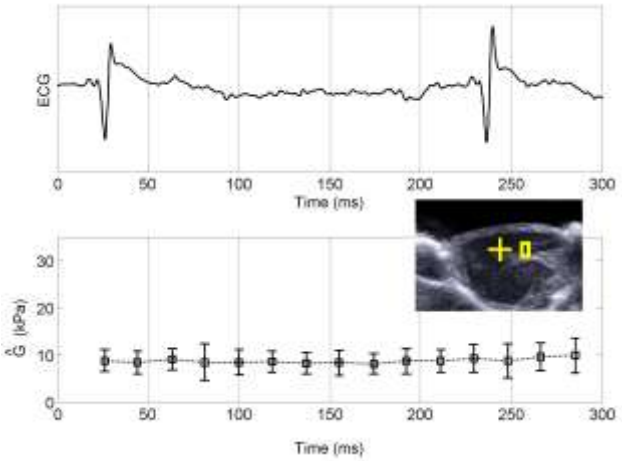

Fig. 10. Electrocardiogramm (top) and $\hat{G}$ (bottom) as a function of time. Insert- Position of the focal point (yellow cross) and of the ROI (yellow rectangle).

an estimation of Gd at 400Hz. In agreement with the expected effect of shear viscosity, values from the work of Vappou et al [11] who were working with MRE at a lower frequency (180Hz) are lower. They found an average value of 8.45 kPa for the storage modulus Gd in the rat brain and a range of 0 to 16 kPa was given for their elasticity map. With an excitation at higher frequency (1200 Hz), Atay et al [10] found average values for the shear modulus ranging from 12 to 19 kPa in different thick slices (anterior/middle/posterior) of the mouse brain, which is higher than the average values found here for similar slices ($\hat{G}$ = 13.2 +/- 0.7 kPa for the forebrain and $\hat{G}$ = 11.7 +/- 0.6 kPa for the midbrain). This is in agreement with the frequency dependent dispersion of shear wave speed. In future work, it would be of great interest to perform Shear Wave Spectroscopy [27] in order to measure the dispersion curve and so to quantify both shear viscosity and elasticity of brain tissues simultaneously.

Perhaps of greater interest than the average shear modulus, an interesting result is the high contrast of elasticity values found in the brain. The good resolution of elasticity maps allows identification of small structures that are reproducible for all animals. This is a key point for the development of a real-time imaging technique able to distinguish different anatomical regions in the brain. In particular, the forebrain appears stiffer than the midbrain. This observation is consistent with the literature. In their work on the mouse brain in vivo by MRE, Atay et al [10] compared the mean dynamic shear modulus obtained in the anterior, middle and posterior part of the brain and found that the anterior part is stiffer. Vappou et al [11] published an elasticity map of the rat brain realized with in vivo MRE that also shows higher stiffness in the forebrain.

Possible sources of errors in the shear modulus quantification have to be discussed. As explained in the Materials and Methods section, the artifacts that could be induced by reflections or low SNR were taken into account in the data processing. One source of error comes from the fact that the approximation of low viscosity is not true. The literature shows that G_l is non-negligible compared to G_d in brain tissues, which can lead to an overestimation of G_d by our technique. This issue can be assessed in future work by measuring both G_d and G_l using Shear Wave Spectroscopy [27]. Secondly, tissue attenuation has the effect of shifting the spectrum of the shear wave to the lower frequencies during the propagation. However, the shift of the central frequency was measured to be lower than 10% and in each pixel the estimation of the shear wave speed is averaged from different sources, so we consider this effect negligible. The main possible source of error in the quantification comes from the segmentation and registration processes, particularly for small ROIs. A small misalignment between maps can have a non-negligible impact next to the margins between different brain parts. This was minimized by selecting ROIs smaller than the region considered, but it could explain why higher variations were found in the smaller ROIs i.e. the two white matter regions. Finally, the complex geometry of brain structures could also locally have an impact on the shear wave propagation and so add variability in the shear modulus quantification.

A significant result of the present study is that some brain tissues exhibit an anisotropic behavior for shear wave propagation. By studying shear wave propagation in both sagittal and coronal directions, a method for the assessment of brain shear anisotropy is proposed. The resulting relative shear anisotropy map clearly exhibits links with anatomical regions. In particular, in the five ROIs studied, both white matter regions are highly anisotropic when the three gray matter regions exhibit similar shear modulus values for both scans. This strong anisotropy could be a consequence of the orientation of the axonal fibers. Indeed, in muscle, it is well known that the propagation of the shear waves is different along the muscle fibers than in the transverse section [22, 28, 29]. In this study, only two directions are measured. To verify the hypothesis of a correlation between shear anisotropy and fiber orientation, these preliminary results need to be extended by scanning the brain in multiple orientations in order to thoroughly measure the 3D elasticity tensor and compare the results with Diffusion Tensor Imaging (DTI).

There is no consensus to date in the literature on whether gray matter or white matter is stiffer. For humain brain, some MRE studies reported higher values of elasticity in white matter than in gray matter (McCraken et al [9], Kruse et al [6]). On the other hand, Green et al [5] found gray matter stiffer than white matter but it is noticeable that their values were very close for both tissue types and much lower than those reported in other MRE studies. In the present study with SWI, we found that the white matter regions studied are anisotropic and so we conclude that a thorough study of the 3D elasticity tensor is needed to answer this question.

Even if invasive, this new technique is promising both for intra-operative clinical applications and medical research on small animals. If pathological brain tissues do have impaired mechanical properties, our method could be used to monitor treatment efficiency or to follow and better understand the progression of diseases on animal models. Concerning transition to clinical use, this technique could rapidly be evaluated intra-operatively in the context of surgery of brain lesions. Promising results for brain tumor localization and lesion margins assessment were obtained recently in a preliminary clinical study during brain surgery [30, 31]. Research on adaptive ultrasonic focusing techniques is also in progress [32-35] to make transcranial ultrasound elastography of the brain possible in the near future.

REFERENCES

[1] S. Cheng, E. C. Clarke, and L. E. Bilston, “Rheological properties of the tissues of the central nervous system: a review.” Med Eng Phys, vol. 30, no. 10, pp. 1318–1337, Dec 2008.

[2] S. Nicolle, M. Lounis, R. Willinger, and J.-F. Palierne, “Shear linear behavior of brain tissue over a large frequency range.” Biorheology, vol. 42, no. 3, pp. 209–223, 2005.

[3] S. Papazoglou, C. Xu, U. Hamhaber, E. Siebert, G. Bohner, R. Klingebiel, J. Braun, and I. Sack, "Scatter-based magnetic resonance elastography." Phys Med Biol, vol. 54, no. 7, pp. 2229–2241, Apr 2009.
[4] I. Sack, B. Beierbach, J. Wuerfel, D. Klatt, U. Hamhaber, S. Papazoglou, P. Martus, and J. Braun, "The impact of aging and gender on brain viscoelasticity." Neuroimage, vol. 46, no. 3, pp. 652–657, Jul 2009.
[5] M. A. Green, L. E. Bilston, and R. Sinkus, "In vivo brain viscoelastic properties measured by magnetic resonance elastography." NMR Biomed, vol. 21, no. 7, pp. 755–764, Aug 2008.
[6] S. A. Kruse, G. H. Rose, K. J. Glaser, A. Manduca, J. P. Felmlee, C. R. Jack, and R. L. Ehman, "Magnetic resonance elastography of the brain." Neuroimage, vol. 39, no. 1, pp. 231–237, Jan 2008.
[7] D. Klatt, U. Hamhaber, P. Asbach, J. Braun, and I. Sack, "Noninvasive assessment of the rheological behavior of human organs using multifrequency mr elastography: a study of brain and liver viscoelasticity." Phys Med Biol, vol. 52, no. 24, pp. 7281–7294, Dec 2007.
[8] I. Sack, B. Beierbach, U. Hamhaber, D. Klatt, and J. Braun, "Non-invasive measurement of brain viscoelasticity using magnetic resonance elastography." NMR Biomed, vol. 21, no. 3, pp. 265–271, Mar 2008.
[9] P. J. McCracken, A. Manduca, J. Felmlee, and R. L. Ehman, "Mechanical transient-based magnetic resonance elastography." Magn Reson Med, vol. 53, no. 3, pp. 628–639, Mar 2005.
[10] S. M. Atay, C. D. Kroenke, A. Sabet, and P. V. Bayly, "Measurement of the dynamic shear modulus of mouse brain tissue in vivo by magnetic resonance elastography." J Biomech Eng, vol. 130, no. 2, p. 021013, Apr 2008.
[11] J. Vappou, E. Breton, P. Choquet, R. Willinger, and A. Constantinesco, "Assessment of in vivo and post-mortem mechanical behavior of brain tissue using magnetic resonance elastography." J Biomech, vol. 41, no. 14, pp. 2954–2959, Oct 2008.
[12] B. Larrat, Q. C. Chan, X. F. Yang, G. Li, E. S. Yang, M. Fink, and R. Sinkus, "Anisotropic viscoelastic properties of the corpus callosum - application of high-resolution 3d mr-elastography to an alzheimer mouse model," in Proc. IEEE Ultrasonics Symposium, Oct. 28–31, 2007, pp. 676–679.
[13] R. Muthupillai, D. J. Lomas, P. J. Rossman, J. F. Greenleaf, A. Manduca, and R. L. Ehman, "Magnetic resonance elastography by direct visualization of propagating acoustic strain waves." Science, vol. 269, no. 5232, pp. 1854–1857, Sep 1995.
[14] S. Catheline, J. L. Thomas, F. Wu, and M. A. Fink, "Diffraction field of a low frequency vibrator in soft tissues using transient elastography." IEEE Trans Ultrason Ferroelectr Freq Control, vol. 46, no. 4, pp. 1013–1019, 1999.
[15] L. Sandrin, M. Tanter, J.-L. Gennisson, S. Catheline, and M. Fink, "Shear elasticity probe for soft tissues with 1-d transient elastography." IEEE Trans Ultrason Ferroelectr Freq Control, vol. 49, no. 4, pp. 436–446, Apr 2002.
[16] M. Tanter, J. Bercoff, L. Sandrin, and M. Fink, "Ultrafast compound imaging for 2-d motion vector estimation: application to transient elastography." IEEE Trans Ultrason Ferroelectr Freq Control, vol. 49, no. 10, pp. 1363–1374, Oct 2002.
[17] J. Bercoff, S. Chaffai, M. Tanter, L. Sandrin, S. Catheline, M. Fink, J. L. Gennisson, and M. Meunier, "In vivo breast tumor detection using transient elastography." Ultrasound Med Biol, vol. 29, no. 10, pp. 1387–1396, Oct 2003.
[18] A. P. Sarvazyan, O. V. Rudenko, S. D. Swanson, J. B. Fowlkes, and S. Y. Emelianov, "Shear wave elasticity imaging: a new ultrasonic technology of medical diagnostics." Ultrasound Med Biol, vol. 24, no. 9, pp. 1419–1435, Nov 1998.
[19] J. Bercoff, M. Tanter, and M. Fink, "Supersonic shear imaging: a new technique for soft tissue elasticity mapping." IEEE Trans Ultrason Ferroelectr Freq Control, vol. 51, no. 4, pp. 396–409, Apr 2004.
[20] M. Tanter, J. Bercoff, A. Athanasiou, T. Deffieux, J.-L. Gennisson, G. Montaldo, M. Muller, A. Tardivon, and M. Fink, "Quantitative assessment of breast lesion viscoelasticity: initial clinical results using supersonic shear imaging." Ultrasound Med Biol, vol. 34, no. 9, pp. 1373–1386, Sep 2008.
[21] M. Muller, J.-L. Gennisson, T. Deffieux, M. Tanter, and M. Fink, "Quantitative viscoelasticity mapping of human liver using supersonic shear imaging: preliminary in vivo feasibility study." Ultrasound Med Biol, vol. 35, no. 2, pp. 219–229, Feb 2009.
[22] J.-L. Gennisson, T. Deffieux, E. Macé, G. Montaldo, M. Fink, and M. Tanter, "Viscoelastic and anisotropic mechanical properties of in vivo muscle tissue assessed by supersonic shear imaging." Ultrasound Med Biol, vol. 36, no. 5, pp. 789–801, May 2010.
[23] M. Couade, M. Pernot, M. Tanter, C. Prada, E. Messas, and M. Fink, "Non-invasive quantitative imaging of arterial wall elasticity using supersonic shear imaging," in 2008 IEEE ULTRASONICS SYMPOSIUM, VOLS 1-4 AND APPENDIX, ser. ULTRASONICS SYMPOSIUM, 2008, Proceedings Paper, pp. 946–949.
[24] M. Tanter, D. Touboul, J.-L. Gennisson, J. Bercoff, and M. Fink, "High-resolution quantitative imaging of cornea elasticity using supersonic shear imaging." IEEE Trans Med Imaging, vol. 28, no. 12, pp. 1881–1893, Dec 2009.
[25] P. Asbach, D. Klatt, U. Hamhaber, J. Braun, R. Somasundaram, B. Hamm, and I. Sack, "Assessment of liver viscoelasticity using multifrequency mr elastography." Magn Reson Med, vol. 60, no. 2, pp. 373–379, Aug 2008.
[26] J. McLaughlin and D. Renzi, "Using level set based inversion of arrival times to recover shear wave speed in transient elastography and supersonic imaging," Inverse Problems, vol. 22, no. 2, pp. 707–725, Apr 2006.
[27] T. Deffieux, G. Montaldo, M. Tanter, and M. Fink, "Shear wave spectroscopy for in vivo quantification of human soft tissues visco-elasticity." IEEE Trans Med Imaging, vol. 28, no. 3, pp. 313–322, Mar 2009.
[28] S. A. Kruse, J. A. Smith, A. J. Lawrence, M. A. Dresner, A. Manduca, J. F. Greenleaf, and R. L. Ehman, "Tissue characterization using magnetic resonance elastography: preliminary results." Phys Med Biol, vol. 45, no. 6, pp. 1579–1590, Jun 2000.
[29] S. Papazoglou, J. Rump, J. Braun, and I. Sack, "Shear wave group velocity inversion in mr elastography of human skeletal muscle." Magn Reson Med, vol. 56, no. 3, pp. 489–497, Sep 2006.
[30] A. Chakraborty, G. Berry, J. Bamber, and N. Dorwald, "Intra-operative ultrasound elastography and registered magnetic resonance imaging of brain tumors: a feasibility study," Ultrasound, vol. 14, no. 1, pp. 43–49, Feb 2006.
[31] C. Uff, L. Garcia, J. Fromageau, and J. Bamber, "Real time ultrasound elastography in neurosurgery," in Proc. International Symposium of IEEE Ultrasonics, 2009.
[32] S. W. Smith, K. Chu, S. F. Idriss, N. M. Ivancevich, E. D. Light, and P. D. Wolf, "Feasibility study: real-time 3-d ultrasound imaging of the brain." Ultrasound Med Biol, vol. 30, no. 10, pp. 1365–1371, Oct 2004.
[33] G. Montaldo, M. Tanter, and M. Fink, "Real time inverse filter focusing through iterative time reversal." J Acoust Soc Am, vol. 115, no. 2, pp. 768–775, Feb 2004.
[34] F. Vignon, J. F. Aubry, M. Tanter, A. Margoum, and M. Fink, "Adaptive focusing for transcranial ultrasound imaging using dual arrays." J Acoust Soc Am, vol. 120, no. 5 Pt 1, pp. 2737–2745, Nov 2006.
[35] M. Pernot, J.-F. Aubry, M. Tanter, A.-L. Boch, F. Marquet, M. Kujas, D. Seilhean, and M. Fink, "In vivo transcranial brain surgery with an ultrasonic time reversal mirror." J Neurosurg, vol. 106, no. 6, pp. 1061–1066, Jun 2007.

First A. Author (M'76–SM'81–F'87) and the other authors may include biographies at the end of regular papers. Biographies are often not included in conference-related papers. This author became a Member (M) of IEEE in 1976, a Senior Member (SM) in 1981, and a Fellow (F) in 1987. The first paragraph may contain a place and/or date of birth (list place, then date). Next, the author's educational background is listed. The degrees should be listed with type of degree in what field, which institution, city, state, and country, and year degree was earned. The author's major field of study should be lower-cased.

The second paragraph uses the pronoun of the person (he or she) and not the author's last name. It lists military and work experience, including summer and fellowship jobs. Job titles are capitalized. The current job must

have a location; previous positions may be listed without one. Information concerning previous publications may be included. Try not to list more than three books or published articles. The format for listing publishers of a book within the biography is: title of book (city, state: publisher name, year) similar to a reference. Current and previous research interests end the paragraph.

The third paragraph begins with the author's title and last name (e.g., Dr. Smith, Prof. Jones, Mr. Kajor, Ms. Hunter). List any memberships in professional societies other than the IEEE. Finally, list any awards and work for IEEE committees and publications. If a photograph is provided, the biography will be indented around it. The photograph is placed at the top left of the biography. Personal hobbies will be deleted from the biography.